A numerical study of the dynamics and statistics of single electron systems

L. R. C. Fonseca[a)]
Department of Applied Mathematics and Statistics, State University of New York, Stony Brook, New York 11794-3600

A. N. Korotkov and K. K. Likharev
Department of Physics, State University of New York, Stony Brook, New York 11794-3800

A. A. Odintsov[b)]
Electrotechnical Laboratory, 1-1-4 Umezono, Tsukuba-shi, Ibaraki 305, Japan

(Received 2 February 1995; accepted for publication 30 May 1995)

We describe a new and efficient method for the numerical study of the dynamics and statistics of single electron systems presenting arbitrary combinations of small tunnel junctions, capacitances, and voltage sources. The method is based on numerical solution of a linear matrix equation for the vector of probabilities of various electric charge states of the system, with iterative refining of the operational set of states. The method is able to describe very small deviations from the "classical" behavior of a system, due to the finite speed of applied signals, thermal activation, and macroscopic quantum tunneling of charge (cotunneling). As an illustration, probability of dynamic and static errors in two single electron memory cells with 6 and 8 tunnel junctions have been calculated as a function of bias voltage, temperature, and switching speed. © *1995 American Institute of Physics.*

I. INTRODUCTION

During the past decade several devices using correlated tunneling of single electrons have been suggested and tested.[1–3] These devices consist of one or several small conducting electrodes ("islands"), separated from each other and from external electrodes by tunnel junctions. Despite their very small (submicron) size, each island typically contains billions of background electrons. The electric charge of those electrons is, however, completely compensated by that of crystal lattice nuclei. As a result of the very small capacitance of the islands and junctions, if one more electron tunnels into (out of) an island, the electrostatic potential of the island may change considerably, affecting the tunneling of the following electrons. Such a single electron charging makes it possible, by proper manipulation of the potentials of the external electrodes, to control the motion of single electrons/holes. These single electron devices may be used in various analog and digital systems, in particular in circuits of the so-called Single Electron Logic (SEL),[4–7] where information bits are coded by the presence/absence of extra single electrons in particular islands. The implementation of this idea may open a way to "ultimate" electronics with previously unattainable circuit density (and hence integration scale).

A major problem in the design of single electron circuits is an accurate determination of the digital error probability. Such an error (a misplacement of a single electron in the circuit), may be due to several factors, including thermal activation, finite speed of externally applied signals, and macroscopic quantum tunneling of charge (cotunneling).[2,3] For a circuit of any reasonable complexity, these factors are intractable analytically. This is why several computer algorithms have been developed to analyze complex single electron circuits numerically.

MOSES, developed by Chen *et al.*,[8] is based on a Monte Carlo method[9] and can simulate electron propagation. Its ability to analyze arbitrary circuits consisting of tunnel junctions, capacitances, resistors, and signal sources makes MOSES a convenient tool in the study of the dynamics of single electron systems where rare events are not important. As far as rare events (such as errors) are concerned, two programs have been mentioned in the literature. Pothier[10] has developed a code to calculate rare errors due to cotunneling in a specific device ("the single electron pump") at zero dc voltage and zero temperature. Another program, due to Jensen and Martinis,[11] has been designed to handle more general circuits. Although the results described in that paper are in good agreement with analytic calculations for simple circuits, a detailed analysis of the algorithm has not been provided, making it impossible to reproduce the results and understand the limitations of the program. Besides, several restrictions on the set of states imposed in that work (e.g. exclusion of "shake-up" transitions[12]), can hardly be justified *a priori*.

The purpose of this paper is to introduce SENECA (standing for Single Electron NanoElectronic Circuit Analyzer), a new computer algorithm suitable for studies of the dynamics and statistics of single electron devices, including order-of-magnitude calculation of rare errors due to all the phenomena listed above. SENECA can handle single electron circuits consisting of an arbitrary combination of lumped components (excluding resistors at this stage of development), at arbitrary temperature and time dependence of externally applied signals, as long as sufficient computer resource is available.

The paper is organized as follows. In Sec. II we discuss expressions for the single electron tunneling rates and the

a)Electronic mail: fonseca@ams.sunysb.edu
b)Present address: Department of Applied Physics, Delft Univrsity of Technology, Lorentzweg 1, 2628 CJ Delft, The Netherlands.

 0021-8979/95/78(5)/3238/14/$6.00

approximations used for their evaluation. In Sec. III we describe our algorithm in detail. In Sec. IV we present the analysis of an important SEL device, the single electron trap (memory cell with nondestructive readout). Conclusions and discussion of possible improvements are presented in Sec. V.

II. BASIC EQUATIONS

Single electron tunneling is a stochastic phenomenon and its theory can only predict probability rates Γ of the possible tunneling events.[1–3] Hence, two numerical routes are possible in the analysis of single electron devices and circuits. In a Langevin-like route, the rates are used in a Monte Carlo scheme[9] to simulate possible scenarios of electron tunneling between the islands. This is a very convenient method for studying the typical behavior of the electrons in a device. However, in cases when very rare tunneling events of some type (say, those leading to digital errors in SEL devices) take place against the background of much more frequent events of another kind (say, regular operation of these devices), the Monte Carlo method becomes impractical as far as computation time is concerned.

In a Fokker–Planck-like route, probabilities P_i of all possible states of the system (each characterized by a particular charge configuration) are calculated by the master equation,[2] which may be written in either scalar or matrix form:

$$\frac{dP_i}{dt}=\sum_j \Gamma_{ji}P_j-\sum_j \Gamma_{ij}P_i \quad \text{or} \quad \frac{d\mathbf{P}}{dt}=\mathbf{\Gamma P}, \tag{1}$$

where Γ_{ij} is the rate of transition between states i and j, $\Gamma_{ij}=\Gamma_{ji}$ and $\Gamma_{ii}=-\Sigma_{j\neq i}\Gamma_{ij}$. Using this approach, it is possible to handle cases when the rates Γ_{ij} of various tunneling events differ drastically, and therefore it is our method of choice. Its apparent drawback, the necessity to store information about all states of the system, can be rectified to a large extent by taking into account the hierarchy of the tunneling rates Γ_{ij}, where only rates higher than a certain threshold value are considered at a time. This approach will be the subject of detailed discussion in the next section; before that, we shall concentrate on the rates Γ_{ij}.

Consider an arbitrary circuit consisting of conducting islands, connected to each other and to external electrodes by tunnel junctions and/or capacitances. Each junction i is characterized by its capacitance C_i and tunnel conductance G_i. Provided that

$$G_i \ll R_Q^{-1}, \tag{2}$$

where $R_Q=\pi\hbar/2e^2\sim 6.5\ \mathrm{k\Omega}$ is the resistance quantum, the instant state of the circuit is completely characterized by a particular configuration of extra charges on the islands. In the limit (2), the quasiclassical "orthodox" theory of single electron tunneling[5] says that an electron can only tunnel through one junction at a time, and that tunneling of an electron through junction n has the probability rate

$$\Gamma=\frac{2\pi}{\hbar}\,\alpha_i\frac{\Delta E}{\exp\left(\dfrac{\Delta E}{k_BT}\right)-1}, \tag{3}$$

where $\alpha_i=G_iR_Q/\pi^2\ll 1$, and ΔE is the difference between the final and initial values of the electrostatic energy of the system. According to this formula, at zero temperature the tunneling is only possible if $\Delta E<0$, i.e., electrons only travel in the direction of lower potential energy. At finite temperatures, tunneling in the reverse direction is also possible due to thermal activation, but at $k_BT\ll\Delta E$ the rate of these thermally induced events is exponentially low.

Quantum tunneling through $N>1$ junctions at a time, or "cotunneling," is also possible,[13] though typically at a much lower rate than that of the "classical" tunneling through one junction. For finite temperature, the rate of an Nth-order "inelastic" cotunneling process[14] is given by the expression[13,15]

$$\Gamma^{(N)}=\frac{2\pi}{\hbar}\left(\prod_{i=1}^{N}\alpha_i\right)\int_0^\infty S^2(\omega_1,\ldots,\omega_{2N})\times\delta\left(\Delta E_N+\sum_{i=1}^{2N}\omega_i\right)\prod_{i=1}^{2N}(1-f(\omega_i))\,d\omega_i. \tag{4}$$

In expression (4), $\Delta E_N=E_N-E_0$ is the change in the electrostatic energy during cotunneling from the initial state 0 to the final state N, f is the Fermi function, and the function S is defined as

$$S(\omega_1,\ldots,\omega_{2N})=\sum_{\mathrm{perm}\{k_1,\ldots,k_N\}}\prod_{k=1}^{N-1}\frac{1}{\varepsilon_k}, \tag{5}$$

where ε_k are increments in the total energy of the system,

$$\varepsilon_k=\Delta E_k+\sum_{l=1}^{k}(\omega_{2l-1}+\omega_{2l}). \tag{6}$$

In relation (6), $\Delta E_k=E_k-E_0$ is the change in the electrostatic energy during cotunneling from initial state 0 to intermediate state k, $\omega_{2l-1}+\omega_{2l}$ is the energy of one of the k electron-hole excitations created between states 0 and k, and the permutation is taken over all possible sequences of intermediate states. Equation (4) expresses the fact that the quantum-mechanical amplitudes of all the cotunneling sequences with the same initial and final states should be added coherently to give the total rate of the resulting cotunneling process (which will be called a "transition").

In most cases, a final state of practical interest can only be accessed by transitions in order higher than a certain number N, because all the lower order transitions would raise the energy of the system. Moreover, due to the smallness of α_i (2), the rate of the transition of the lowest possible order usually dominates. In some cases, however, the coexistence of transitions of different orders leading to the same final state must be considered as their probability rates may be comparable (we will return to this issue later).

The multi-dimensional integral (4) can be calculated analytically for a very limited number of cases.[13,16] In general, only a numerical calculation is possible, which may be extremely time consuming since it is a $(2N)$th order integration. An approximation can be obtained in the limit when the final energy difference $|\Delta E_N|$ is much smaller than some threshold value $|\Delta E_{\mathrm{th}}|$ (if $|\Delta E_N|>|\Delta E_{\mathrm{th}}|$, a lower order transition is possible even at $T=0$). In this case, the excitation energies $\omega_{2l-1}+\omega_{2l}$ may be taken to be zero, and expression

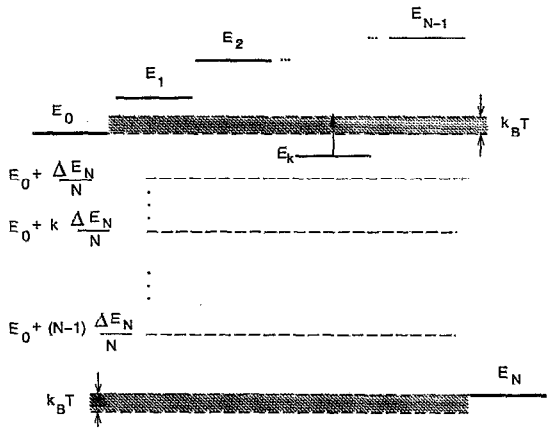

FIG. 1. A typical distribution of electrostatic energies E_k (solid lines) and their singularity levels $E_0+k\Delta E_N/N$ (dashed lines) for an Nth order cotunneling between states 0 and N. Within the framework of the exclusion principle, such a process is forbidden because the level E_k ($k<N$) is between E_0 and E_N, and hence the kth order cotunneling from state 0 to state k is possible. In order to make a better approximation, we take the Nth order process into account as well, but shift E_k (arrow) beyond the nearest border of the interval $[E_0+k_BT,E_N-k_BT]$ to avoid the divergence.

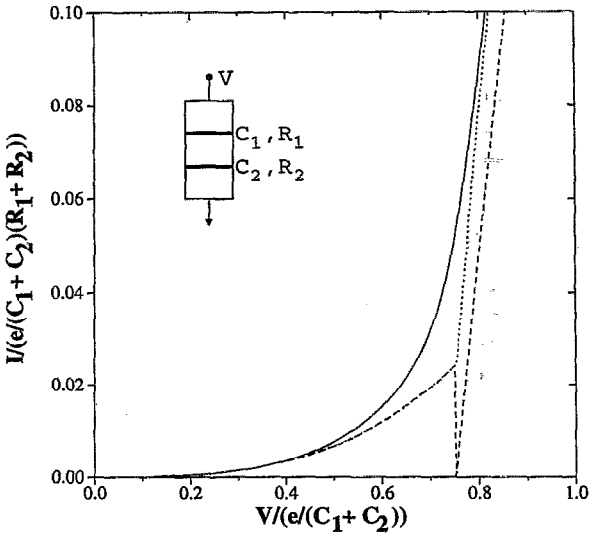

FIG. 2. Direct current $I-V$ curves of a single electron transistor (inset) with $C_2=2C_1$, $\alpha_2=2\alpha_1=0.5$, and zero background charge, at $T=0$. Solid line: calculation using the exact formula (Ref. 17). Dashed line: calculation using the Jensen–Martinis approximation with the exclusion of cotunneling at the threshold voltage. Dotted line: the similar approximation with the energy shift at the threshold.

(4) can be integrated analytically.[13] A better approximation (due to Jensen and Martinis[11]) is to replace arbitrary electron-hole excitation energies by fixed values equidistant on the interval $[0,\Delta E_N]$, i.e.

$$\omega_{2l-1}+\omega_{2l}=-\frac{\Delta E_N}{N}. \tag{7}$$

Using relation (7), the expression for $\Gamma^{(N)}$ can be calculated analytically and the result is:[11]

$$\Gamma^{(N)}=\frac{2\pi}{\hbar}\left(\prod_{i=1}^{N}\alpha_i\right)S^2F_N(\Delta E_N,T), \tag{8}$$

where

$$S=\sum_{\mathrm{perm}\{j_1,\ldots,j_N\}}\left(\prod_{k=1}^{N-1}\frac{1}{\Delta E_k-\frac{k}{N}\Delta E_N}\right), \tag{9}$$

$$F_N(\Delta E_N,T)=\frac{\Pi_{i=1}^{N-1}[(2\pi k_BTi)^2+(\Delta E_N)^2]}{(2N-1)!}\frac{\Delta E_N}{\exp\left(\frac{\Delta E_N}{k_BT}\right)-1}. \tag{10}$$

Formally, the perturbative result (4) diverges if there are states with energies E_k in the window $E_N\leqslant E_k\leqslant E_0$, of which the divergence of (9) for $\Delta E_k=(k/N)\Delta E_N$ is a consequence (Fig. 1). According to the earlier approximation,[11–13] cotunneling processes with intermediate energies in that window should not be considered at all. We will call this assumption the "exclusion principle."

In the limit $\alpha\ll 1$, the exclusion principle is valid for almost all parameter values. The width of the coexistence region, where the rates of transitions of different orders are comparable, goes to zero as α does. For real systems, however, α is finite and the width of the coexistence region scales as $\alpha^{1/(2N-3)}$, growing rapidly with the order of transition N. Disregard of the higher order transitions at finite α may result in unphysical jumps of the rates (by many orders of magnitude) at the transition thresholds. For example, Figure 2 shows the dc I-V curves of a simple system, the single electron transistor,[1–3] where transitions can only have orders $N=1$ (classical tunneling) and $N=2$ (cotunneling) for a particular choice of parameters. One can see that the exclusion of the cotunneling beyond the threshold for the classical transition leads to a jump in the current down to zero, while in reality it grows monotonically.

Presently, there is no complete theoretical description for the behavior of an arbitrary single electron system in the coexistence region, despite some recent progress in this direction.[17–20] Under these circumstances, we have accepted what we believe to be the most natural assumption, i.e. the independent coexistence of incoherent transitions of different orders, with rates calculated in the Jensen–Martinis approximation (8)–(10). We call this assumption the "coexistence principle." In order to avoid the singularities discussed above, each electrostatic energy level $E_k=E_0+\Delta E_k$ which falls inside interval $E_N\leqslant E_k\leqslant E_0$ is formally shifted to the nearest border of this interval (Fig. 1). This shift circumvents divergencies and produces a smooth transition from one dominating order to the next. However, a divergence of a different kind may appear when $E_N\to E_0$ and the temperature is finite. In this case, Eq. (10) gives a finite result, $F_N(0,T)\propto T^{2N-1}$, but S in Eq. (9) diverges as soon as the three energies E_0, E_k and E_N become aligned (this situation resembles the resonant tunneling divergence). In order to avoid this divergence, we add two "buffer zones" of width k_BT to the interval $[E_0, E_N]$, as shown in Fig. 1: if any $E_k\in[E_0, E_N]$, then E_k is formally shifted to the top of the

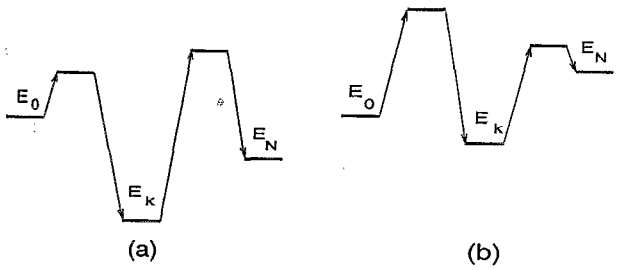

FIG. 3. "Shake-up" processes $E_0 \rightarrow E_N$ via an intermediate state E_k, which are possible at (a) $T=0$ and (b) $T>0$.

upper buffer zone or to the bottom of the lower buffer zone, whichever is closest. As a result, $\Gamma^{(N)}(\Delta E_N, T=0) \propto -\Delta E_N$ and $\Gamma^{(N)}(\Delta E_N=0,T) \propto T$.

Figure 2 compares the current calculated using the coexistence and exclusion principles with the exact current for the single electron transistor[17] at $T=0$. The improvement in the ratio $I_{\text{exact}}/I_{\text{calc}}$ is quite good: at the threshold it changes from infinity to ~ 2 as we switch from the exclusion principle to our approach. Although the difference between our result and the exact calculation still seems considerable, the reader should remember that, in most cases, the probabilities of rare events in typical circuits (see Sec. IV) change by orders of magnitude due to a small change of parameters. In those cases, the accuracy of our approach corresponds to a negligible change of parameters, and it seems sufficient for all present-day applications.

In addition to the usual transitions where all the intermediate energies E_k lie above $\max\{E_0, E_N\}$, our approach also allows a natural account of the so-called "shake-up" transitions,[12] where $E_k < \min\{E_0, E_N\}$ (Fig. 3). The intermediate states of the shake-ups are accessible via lower order transitions starting from the initial state, and hence they are neglected in schemes using the exclusion principle.

Even in the approximation (8), the exact calculation of the cotunneling rates is a time consuming task, because the number of parameters (intermediate energies) necessary to evaluate $\Gamma^{(N)}$ scales as $N!$. Since we sometimes need fast estimates of the cotunneling rates (before their exact calculation), we use the following definition:

$$\Gamma^{(N)}_{\text{est}} \equiv \frac{2\pi}{\hbar} \alpha^N S^2_{\text{est}} F_N(\Delta E_N, T), \tag{11}$$

where

$$S_{\text{est}} = \left(\frac{2NC}{e^2}\right)^{N-1} \frac{N}{(N-1)!}. \tag{12}$$

Expression (12) is exactly valid[11] for cotunneling through a simple 1D array of N similar tunnel junctions, if the only capacitances taken into account are those between the closest neighbor islands: $C_{i,i+1}=C$. It also presents a reasonable order-of-magnitude approximation for most single electron circuits of interest, which typically include one or several 1D arrays as their major components (see Sec. IV below). If this is not the case, C should be considered as a free parameter used for tuning the algorithm.

III. THE ALGORITHM

A. Introductory remarks

In principle, an algorithm based on solution of Eq. (1) should take into account all possible charge states resulting from both classical and cotunneling transitions in some range of the involved parameters. For single electron devices and systems of current interest (with the number M of islands ranging from 5–6 to 20–30), handling of all possible states and paths between them is impossible. Indeed, if we consider only charge configurations consisting of islands with one electron or one hole or none of these (an empty island), which is the usual case at a moderate voltage and temperature, the number of states scales as $2^{3M/2}$, while the number of paths connecting these states scales as 2^{3M}.

Nevertheless, when the temperature and the tunnel conductances are small (2), most of the possible transitions (either those leading to an increase in the electrostatic energy, or those of high cotunneling order) have very low rates. As a consequence, a large number of charge states have very low probabilities P (below a certain threshold P_{th}) and may be ignored. Hence, we chose an iterative approach which considers only a limited number of states in each iteration, adding to the list of states only new ones which have an estimated probability P_{est} that satisfies the condition

$$P_{\text{est}} > P_{\text{th}}(n). \tag{13}$$

Those states may lead to new generations of states, but our experience shows that the iterations rapidly converge in all cases of interest.

An algorithm developed to analyze real circuits should describe the time evolution of the system. In fact, the problems we want to address always involve a certain time interval ζ. For example, if we want to determine the probability of error during storage of information in a single electron memory cell, we may start the calculation with a certain charge state (one extra electron inside the cell) at $t=0$ and observe how error probability grows with time. In this case, the externally applied voltages are usually constant. Another example involves errors created when the memory cell is switched from one state to another by an external signal. If the switching signal speed is too high, the electron may stay in the initial state, and we should calculate the probability of such an outcome which is regarded as an error.

In either case, the description of the system should be uniform in time, meaning that the selection rule defined by Eq. (13) should be used with the same $P_{\text{th}}(n)$ throughout the time interval ζ.

We will now describe the algorithm level by level, in the direction of increasing detail.

B. The iterative procedure

As was already mentioned, the basic idea of the method is to refine the description of the process by successive iterations $n=0,1,2,\ldots,n_{\max}$. Each iteration corresponds to a passage along the total time interval ζ, subdivided in a number of time steps (Fig. 4). The length Δt of the time step (selected by the user) should be small enough, so that variations

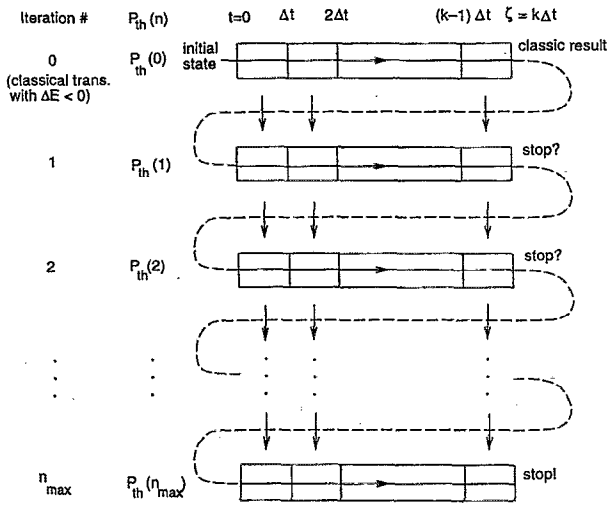

FIG. 4. Schematic description of our algorithm. The solid horizontal arrows represent the program sequence at each iteration, starting with the initial state at $t=0$ and finishing at $t=\zeta$. The dashed lines show that the new iteration starts if no state of interest has been found at the end of the previous iteration. The vertical arrows represent the information transferred between correspondent time steps of adjacent iterations.

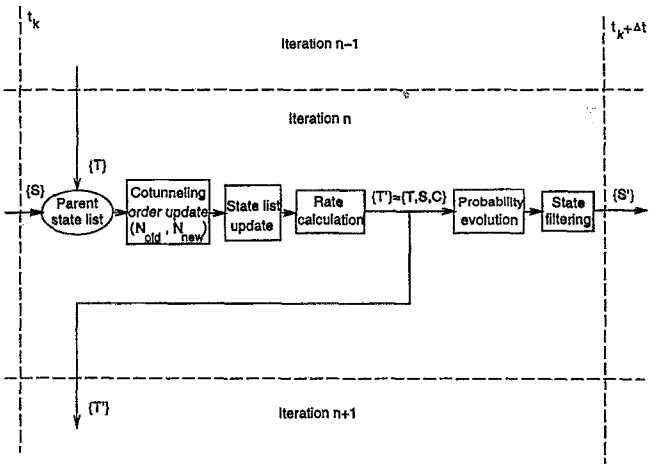

FIG. 5. Block diagram of a time step. The vertical dashed lines separate adjacent time steps considered at the same iteration, while the horizontal dashed lines separate analyses of the same time step in adjacent iterations.

of the external potentials during the step are negligible. The user should also specify the threshold probability $P_{\rm th}$, which is the smallest probability of interest.

In order to reach $P_{\rm th}$ iteratively, we define partial thresholds $P_{\rm th}(n)$, which are the lower bound for the probabilities of the states considered in the nth iteration—see Eq. (13). A natural choice of $P_{\rm th}(n)$ is such that each new iteration roughly corresponds to one more order of cotunneling. Thus $P_{\rm th}(n)$ is defined by the relation

$$P_{\rm th}(n)=\Gamma_{\rm est}^{(n)}\zeta, \tag{14}$$

where $\Gamma_{\rm est}^{(n)}$ is defined by Eq. (11). Equation (11) requires knowledge of ΔE_n. In order to estimate ΔE_n, we consider a subset $\{SS\}$ of the charge states of the system obtained from the addition to the initial charge configuration (determined by the user), of a single electron in some island, plus a single hole in a different island. ΔE_n is defined as one half of the maximum energy difference between all states of this subset. Our numerous experiments with the algorithm have shown that this value of ΔE_n is a good representative of the energy differences between initial and final states, and the above definition of $P_{\rm th}(n)$ allows a reasonable trade-off between the required computer speed and memory to be reached.

Each iteration consists of sequential analyses of the time steps which constitute the time interval ζ. At each time step, the program finds new charge states of the system satisfying Eq. (13) and calculates these probabilities (for details, see below). At the end of each iteration, the program determines if one (or more) of the states with probability above $P_{\rm th}$ at $t=\zeta$ is the rare event of interest.

In the initial passage along the time period ($n=0$), only classical transitions that decrease the energy of the initial state are allowed. In other words, the first passage considers only the classical evolution of the system at zero temperature. Thus, a crude description of the system dynamics is achieved. Classic transitions at finite temperature and cotunneling are considered in the next iterations.

The iterative procedure is stopped if one of the following conditions, checked after each iteration, is fulfilled:

(1) the relative difference between the values of the probability of the state under search, which were found in two consecutive iterations, is less than the accuracy selected by the user (search is completed with a "positive" result);
(2) the current threshold $P_{\rm th}(n)$ drops below[21] the finite threshold $P_{\rm th}$ and no state of interest is found (search with a "negative" result);
(3) the iteration number n exceeds some threshold $n_{\rm max}$ specified by the user (search with an inconclusive result).

An important feature of our implementation is that some information about each time step is conserved from iteration to iteration (represented by the vertical arrows in Fig. 4). The information includes transition rates, charge configurations, energies and "parent–child" links. Thus, each new iteration adds new transitions to the list created in the previous iterations, and does not recalculate what has already been done.

C. The time step

Each time step starts with the state list update (Fig. 5). At t_k, the list of active charge states contains two parts: the set $\{T\}$ of all states found at the same time step of the previous iteration, and the set $\{S\}$ of states promoted from the previous time step of the current iteration.

The first operation (Fig. 5) is an update of two integer numbers, namely $N_{\rm old}$ and $N_{\rm new}$, prescribed to each state in $\{S\}$ and $\{T\}$. $N_{\rm new}$ is the maximum order of cotunneling in which state i will be used to create new states (or new transitions to old states) in the current time step. Before the update, $N_{\rm new}$ is copied to $N_{\rm old}$, which is the highest order already considered, and is updated as the largest integer N satisfying the following equation:

$$P_{\text{est}} \geqslant P_{\text{th}}(n), \quad P_{\text{est}} = \bar{P}_i \Gamma_{\text{est}}^{(N)} \Delta t, \tag{15}$$

where $\bar{P}_i$ is the state's mean probability. $\Gamma_{\text{est}}^{(N)}$ is again taken from Eq. (11), but in this case ΔE_N is defined as the maximum energy difference between the parent state and all states of the subset $\{SS\}$ defined before. If $N_{\text{new}} > N_{\text{old}}$, the state will be used for the generation of child states in orders $N_{\text{old}}+1,\ldots,N_{\text{new}}$. If, however, $N_{\text{new}} \leqslant N_{\text{old}}$, the state will not be evolved.

Next, using the complete set $\{T,S\}$ of these "parent" states (Fig. 5), the algorithm generates a set of "child" states $\{C\}$ (the details of this generation will be discussed below). In the process of generation of the child states, new transition rates Γ_{ij} are calculated using Eq. (8) and added to the matrix $\boldsymbol{\Gamma}$ (see Eq. (1)), which already contains the rates of transitions between the states in $\{T\}$. Note that the rates Γ_{ij} are evaluated assuming constant external potentials during each time step; we use the values of potentials calculated at the center point of the time step.

After the list $\{T'\}=\{T,S,C\}$ is completed and matrix $\boldsymbol{\Gamma}$ is filled, the operation of probability evolution is performed. It consists of solving the master equation (1) in the interval $[t_k, t_k+\Delta t]$, with initial condition $\mathbf{P}(t_k)$. The initial condition is different from zero only for the states belonging to $\{S\}$, since for those states the vector $\mathbf{P}(t_k)=\mathbf{P}(t_{k-1}+\Delta t)$ was calculated at the end of the previous time step. Equation (1) can be formally integrated:

$$\mathbf{P}(t_k+\Delta t) = \exp(\boldsymbol{\Gamma}\Delta t)\mathbf{P}(t_k). \tag{16}$$

The program uses the Padé approximant method[22] to calculate the matrix $\exp(\boldsymbol{\Gamma}\Delta t)$.

We also calculate the mean probability of each state during the time step,

$$\bar{P} \equiv \frac{1}{\Delta t}\int_{t_k}^{t_k+\Delta t} P(t')dt'. \tag{17}$$

The mean probability is needed because the change of external potentials at the beginning of the time step may give rise to new states with the probability rapidly disappearing (long before the end of the time step). These "flash" states may be quite important as a transition step to states of interest. According to Eq. (1), their contribution at the kth time step is adequately described by the average $\bar{\mathbf{P}}$. In practice, $\bar{\mathbf{P}}$ may be calculated faster not from Eq. (17), but as $\mathbf{R}(t_k+\Delta t)$, where $\mathbf{R}$ is the solution of the matrix equation

$$\frac{d\mathbf{R}}{dt} = \frac{1}{\Delta t}\mathbf{P}, \quad \mathbf{R}(t_k)=0. \tag{18}$$

Technically, Eq. (18) is solved simultaneously with Eq. (1) by means of the $2m\times 2m$ system of equations

$$\frac{d\tilde{\mathbf{P}}}{dt} = \tilde{\boldsymbol{\Gamma}}\tilde{\mathbf{P}}, \tag{19}$$

where

$$\tilde{\mathbf{P}}(t) = \begin{pmatrix} \mathbf{P}(t) \\ \mathbf{R}(t) \end{pmatrix}, \quad \tilde{\mathbf{P}}(t_k) = \begin{pmatrix} \mathbf{P}(t_k) \\ \mathbf{0} \end{pmatrix}, \quad \tilde{\boldsymbol{\Gamma}} = \begin{pmatrix} \boldsymbol{\Gamma} & \mathbf{0} \\ \mathbf{I}/\Delta t & \mathbf{0} \end{pmatrix},$$

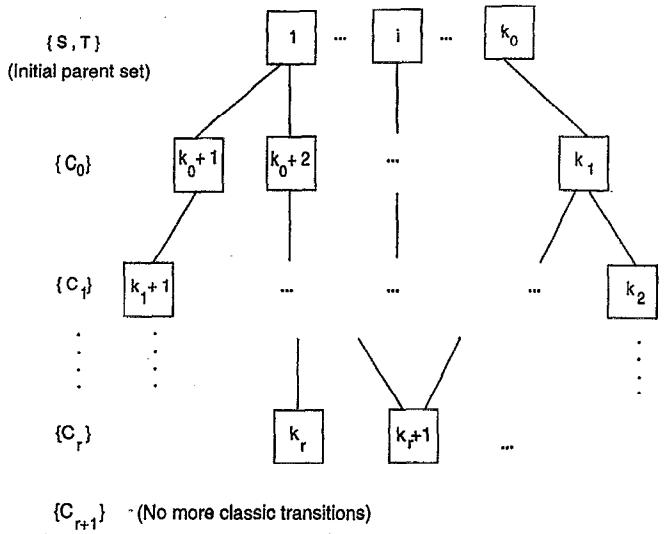

FIG. 6. Different generations of states created during a time step. States of the last set $\{C_r\}$ do not lead to any new states (classically).

and $\mathbf{I}$ is the identity matrix ($\boldsymbol{\Gamma}$ and $\mathbf{I}$ are both $m\times m$ matrices).

The last operation performed in each time step is filtering. It consists of selecting those states of the total set $\{T'\}$, for which the calculated probability $P(t_k+\Delta t)$ is larger than $P_{\text{th}}(n)$. Those filtered states form the set $\{S'\}$ and are promoted to the next time step (Fig. 5).

D. The state list update

The description of a charge state in our program includes its identification number, its electrostatic energy E, current approximations for its probability P and mean probability $\bar{P}$, and the numbers N_{old} and N_{new}. Each "active" state included in the current state list also carries its own list of "passive" states, which are child states that did not satisfy Eq. (13) in the the previous iterations, and thus are not yet included into the active state list (see below). The probabilities of passive states are estimated as P_{est}, using definition (15). Since $P_{\text{th}}(n)$ decreases with the iteration number, passive states have a chance to become active states at each new iteration. This is why we store their charge configurations, energies, and the order of cotunneling in which they were generated. In the following text, "creating a state" means putting all that information together, and including the state into the list of active states.

The state list update at some time step of the nth iteration starts with the parent state list $\{S,T\}$ (Fig. 6), each state carrying its own labels N_{new} and N_{old}. First, old estimates of the probabilities of all passive states (if any) carried by each parent are checked against condition (13). If this condition is satisfied, the passive state is promoted to the list of active states. Second, each parent state is used to create all possible new states accessible through transitions in orders $N_{\text{old}} < N \leqslant N_{\text{new}}$. Since the determination of these cotunneling orders is based on a crude estimate of the maximum energy decrease with relation to each initial state, the actual cotunneling rates may differ from their estimates by several

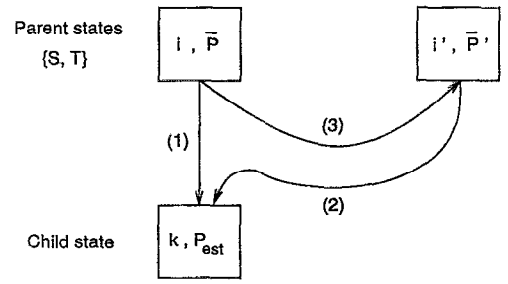

FIG. 7. Three possible scenarios when a new state (k) is generated by a parent state (i): (1) the child state is a new one; (2) the child state coincides with another parent's child state; (3) the child state coincides with an initial parent state $i' \neq i$.

TABLE I. Dependence of a typical SENECA's result on the tuning parameter C (8-junction single electron trap, $T=0$): (A) lifetime of state 0 at $V=-0.8$ mV; (B) the same in a point close to the threshold lifetime $\tau_{th}=\zeta/P_{th}=10^{16}$ s ($V=-1.2$ mV).

$C(10^{-16}$ Farad)	(A) $\tau(10^4$ s)	(B) $\tau(10^{15}$ s)
1	6.3970	5.4543
2	6.3968	5.4543
3	6.3968	3.2794
4	6.3956	3.2794
5	6.3956	3.2794
6	6.3956	3.2794
7	6.3956	3.2794

orders of magnitude depending on the exact energy change. Because of that, once a candidate for a transition is found, its energy E and energy difference to the initial state ΔE_N are calculated exactly, so that $\Gamma_{est}^{(N)}$ may be evaluated more accurately using Eq. (11).

When a charge configuration is determined, one of the following three cases occurs (Fig. 7):

(1) The charge configuration is a new one, i.e. it does not coincide with any parent state or state created previously during the same state list update. In this case, the state's estimated probability P_{est} is obtained using Eq. (15). If Eq. (13) is satisfied, the state is generated and added to the active state list, and the rate is calculated using Eq. (8). Otherwise, the charge configuration (and the remaining information included in the description of a charge state) is stored as a passive state in its parent's passive state list.

(2) The charge configuration coincides with a state (k in Fig. 7), which has been created by another parent state during the same list update. Then, as in the first case, the estimated probability of state k, P_{est}, resulting from the last transition, is calculated using Eq. (15). If relation (13) is satisfied, the exact rate is calculated. No new state is created in this case (since state k already exists), and only the new rate connecting the initial state and state k is recorded. If relation (13) is not satisfied, the charge configuration is stored as a passive state.

(3) The charge configuration coincides with the charge configuration of one of the parent states belonging to $\{S,T\}$. In this case we estimate the correction $\Delta P'_{est}$ to the mean probabilities $\bar{P}'$ and $\bar{P}$ of the parent states due to the new transition, using Eq. (15). If $\Delta P'_{est} > a\bar{P}'$ or $\Delta P'_{est} > a\bar{P}$, then the exact rate is calculated. The factor a, set to 0.01, is a safeguard against a possibly inaccurate estimate $\Delta P'_{est}$. As in the previous case, there is no new state creation, but only the calculation and storage of the exact rate connecting the two states. If the above inequalities are not satisfied, the charge configuration is stored as a passive state, since $\bar{P}$ or $\bar{P}'$ may change from iteration to iteration.

The new states generated by the parent set $\{S,T\}$ are written into the set $\{C_0\}$ (Fig. 6). After all the states in $\{S,T\}$ have concluded their generation procedure, the states in C_0 become the new parent states. The generation procedure is now repeated for the states in $\{C_0\}$, resulting in the set $\{C_1\}$, and so on. However, transitions from $\{C_0\}$ to $\{C_1\}$, from $\{C_1\}$ to $\{C_2\}$, etc., are only allowed in first order, and only if they decrease the energy of the initial state. The reason is that those classic transitions are, in general, much faster (i.e. have higher rates) than cotunneling transitions or classic transitions to states of higher energy—see Eq. (3) and its discussion. In addition, their rates can be calculated very quickly. Higher order processes are left to the next iteration, when N_{new} will be known (for each new state, N_{old} is initialized as zero). Eventually, the classic evolution generates an empty set $\{C_{r+1}\}$, meaning that all states which may result from $\{S,T\}$ in the present iteration have been found, and the state list update is complete.

E. Adjustable parameters

The only adjustable parameter we actively use is C (see Eq. (11)), the effective capacitance value of some homogeneous circuit, somewhat related to the one under analysis. A value of C larger than some optimal C_{opt} means overestimating Γ_{est}. It implies accepting unnecessary transitions that do not substantially change the final result. As a result, computer time is wasted calculating the exact rates of those transitions and solving the master equation (1) with a larger matrix Γ, and memory is overloaded with useless information. On the other hand, a value of C smaller than C_{opt} means underestimating Γ_{est}. In this case, important transitions may be missed, causing the program to converge to a wrong result.

The optimum value C_{opt} may be obtained by trial and error, but our experience has shown that the performance is close to optimal within a relatively broad range around C_{opt}. However, as the order of cotunneling increases, the rate estimate becomes more sensitive to the choice of C and the range narrows down. For example, in the "trap" device described in the next section, the range of optimal values of C includes the average over all closest neighbor capacitances $\bar{C}$, up to some cotunneling order. For higher orders, $\bar{C}$ is no longer included in the optimal range, and C_{opt} may be as high as $2\bar{C}$. Nevertheless, within the optimal range the final result does not change with C by more than a few percent. Table I shows the effect of changing C on the calculated lifetime of state 0. At a typical bias point ($T=0, V_1=-0.8$

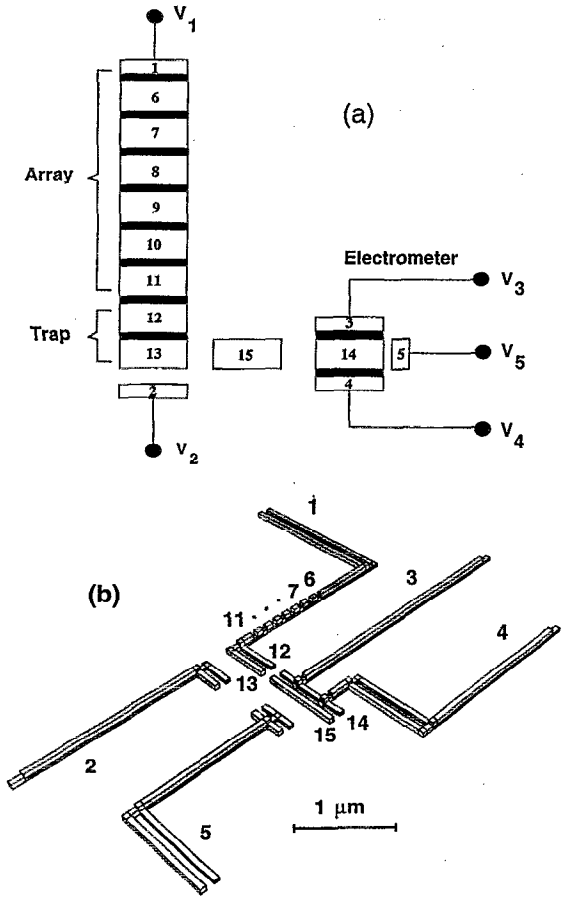

FIG. 8. The 8-junction single electron trap and the monitoring SET electrometer: (a) schematics; (b) geometry used for the calculation of the capacitance matrix.

mV; see Fig. 13), the result is very stable and the optimal range is wide. However, as V_1 decreases and the result approaches the threshold lifetime $\tau_{th}=\zeta/P_{th}$ ($T=0, V=-1.18$ mV), the choice of a small C may yield a wrong result.

Above we have mentioned other parameters (such as $a=0.01$ in the previous section) which in principle may also be altered by the user. Although some of those adjustable parameters can have a strong influence on computer time, memory requirements, and even some influence on the final answer, we have kept them fixed. The reason is that they are all related to C. Thus, the program may be tuned by only changing C, a very convenient feature in practice.

IV. RESULTS

A. The single electron trap

In order to demonstrate the capabilities of SENECA, we analyzed two versions of the simplest SEL circuit, the so-called "single electron trap."[5,23–26] Figure 8(a) shows schematics of the 8-junction trap, together with a single-electron electrometer used for measurement of the charge which may be trapped in the last island of the array. In the particular experimental implementation we are going to discuss,[25] the role of the trap is in fact played by two larger and strongly coupled islands 12 and 13. The other islands of the array create an energy barrier which may keep the electron trapped for a long period of time (for more than 12 hours in recent experiments[26]). The barrier may be suppressed by the application of a voltage bias between the external electrodes 1 and 2: if V_1 exceeds a threshold V_+ (which depends on V_2), a single electron is injected into the trap; its removal requires V_1 to go below another threshold $V_-<V_+$. In the region $V_-<V_1<V_+$ the circuit is bistable: the additional electron may be either in or out of the trap, depending on its history.

A description of the electrometer can be found in Refs. 1–3. In our examples, the trap-electrometer coupling is weak (5–7%), hence the influence of the electrometer on the trap can be neglected. In our calculations we took $V_3=V_4=V_5=0$ to disable the electrometer, but we took into account its passive capacitive coupling to the trap (in particular, via the isolated island 15), in order to be closer to the real system.[25,26] With the same purpose, we used the capacitance

TABLE II. Capacitance matrix of the 8-junction trap. The capacitances (in units of 10^{-16} Farad) are between the electrodes/islands (left column) and the islands (top row). The symmetric part of the matrix is omitted. Electrode 0 means the common ground (a distant conducting environment).

Elec./ Isl. #	Island number 6	7	8	9	10	11	12	13	14	15
0	4.54×10^{-2}	1.37×10^{-2}	4.52×10^{-2}	1.63×10^{-2}	4.38×10^{-2}	1.24×10^{-2}	1.53×10^{-1}	1.05×10^{-1}	1.44×10^{-1}	1.47×10^{-1}
1	$1.90\times10^{+0}$	2.31×10^{-2}	2.76×10^{-2}	9.72×10^{-3}	1.76×10^{-2}	6.61×10^{-3}	3.11×10^{-2}	2.13×10^{-2}	1.31×10^{-2}	1.51×10^{-2}
2	6.32×10^{-3}	3.23×10^{-3}	8.15×10^{-3}	4.21×10^{-3}	1.09×10^{-2}	5.80×10^{-3}	5.97×10^{-2}	1.16×10^{-1}	2.32×10^{-2}	4.04×10^{-2}
3	2.19×10^{-2}	9.63×10^{-3}	2.00×10^{-2}	8.45×10^{-3}	1.71×10^{-2}	6.91×10^{-3}	4.94×10^{-2}	3.06×10^{-2}	$2.77\times10^{+0}$	9.76×10^{-2}
4	9.01×10^{-3}	4.11×10^{-3}	9.08×10^{-3}	4.01×10^{-3}	8.61×10^{-3}	3.71×10^{-3}	2.64×10^{-2}	2.07×10^{-2}	$2.93\times10^{+0}$	1.27×10^{-1}
5	5.11×10^{-3}	2.52×10^{-3}	5.94×10^{-3}	2.92×10^{-3}	6.92×10^{-3}	3.35×10^{-3}	3.13×10^{-2}	3.85×10^{-2}	5.51×10^{-2}	1.45×10^{-1}
6		$1.90\times10^{+0}$	2.05×10^{-2}	3.21×10^{-3}	5.12×10^{-3}	1.38×10^{-3}	5.59×10^{-3}	2.93×10^{-3}	1.75×10^{-3}	1.73×10^{-3}
7			$1.90\times10^{+0}$	8.95×10^{-3}	3.24×10^{-3}	1.13×10^{-3}	3.18×10^{-3}	1.71×10^{-3}	8.89×10^{-4}	8.91×10^{-4}
8				$1.90\times10^{+0}$	2.07×10^{-2}	3.20×10^{-3}	1.06×10^{-2}	4.67×10^{-3}	2.37×10^{-3}	2.26×10^{-3}
9					$1.90\times10^{+0}$	8.94×10^{-3}	6.37×10^{-3}	2.97×10^{-3}	1.19×10^{-3}	1.16×10^{-3}
10						$1.90\times10^{+0}$	3.12×10^{-2}	8.65×10^{-3}	3.09×10^{-3}	2.90×10^{-3}
11							$1.90\times10^{+0}$	1.23×10^{-2}	1.46×10^{-3}	1.44×10^{-3}
12								$4.28\times10^{+0}$	2.87×10^{-2}	2.53×10^{-2}
13									2.07×10^{-2}	3.32×10^{-2}
14										2.75×10^{-1}

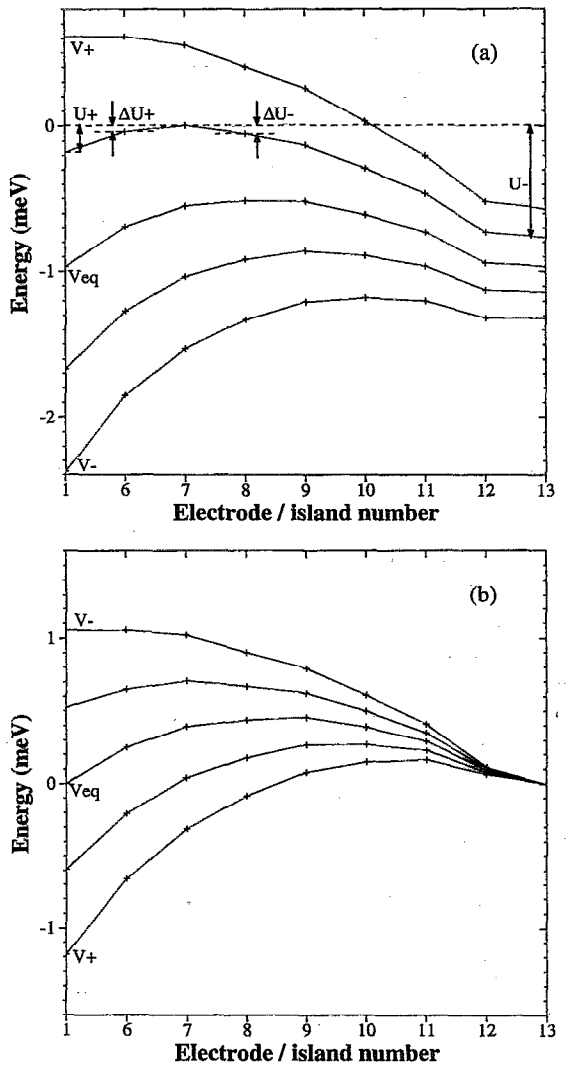

FIG. 9. Energy profiles of the 8-junction trap for several values of V_1 and optimal $V_2=-8.57$ mV: (a) one electron in the array; (b) one hole in the array and one electron in the trap.

matrix C_{ij} calculated[27] using a simplified geometrical model (Fig. 8(b)) of a real experimental device.[25,26] Table II shows the matrix C_{ij} (0 denotes ground) in the "engineering" notation:

$$Q_i=\sum_j C_{ij}(V_i-V_j). \tag{20}$$

The junctions' conductances, taken to be proportional to the junction area S, have the same value $1.07\times10^{-6}\Omega^{-1}$ (except for the larger junction connecting islands 12 and 13, with conductance equal to $2.02\times10^{-6}\Omega^{-1}$). This is a typical experimental value (with the electrodes in the normal state), with the resulting parameters $\alpha_i=0.7\times10^{-3}$.

B. Basic properties

Figure 9(a) shows the profile of the energy barrier created by the array for a single electron entering/leaving the trap (at $T=0$). The change in the profile caused by increasing the potential V_1 leads eventually to the suppression of the barrier, allowing the entrance of an electron into the array at $V_1=V_+$. It is important to note that such an event may occur in various ways. For example, it may be just a sequential tunneling of an electron from the external electrode through the neighboring junctions, as shown in Table III(A). The top curve in Fig. 9(a) corresponds to that scenario. Another possibility for an electron entrance is the creation of an electron-hole pair in the trap, followed by the gradual retreat of the hole, as in Table III(B). Other scenarios are also possible, e.g., the creation of an electron-hole pair in the middle of the array rather than near the trap, though in most cases these scenarios do not provide the lowest energy barrier, at least for the cases we have studied.

If V_1 is decreased, the barrier for the electron exit becomes lower. An expected scenario would be for the electron to exit only after the barrier is completely suppressed (at $T=0$). It turns out, however, that the charge state of the trap is destroyed even before the electron barrier is suppressed, by the entrance of a hole from wire 1 to island 6, and its sequential tunneling into the trap. Figure 9(b) shows the energy barrier for this scenario; it can be seen that the hole barrier is suppressed at $V_1=V_-$, when the electron barrier (Fig. 9(a)) still holds.

One more special value of V_1 is the "equilibrium" potential V_{eq}, where the energies of the system with and without an electron in the trap coincide. From the point of view of possible applications, spontaneous transitions of the system in either direction (empty trap to filled trap and vice versa), are errors. In order to minimize the error rate, the lowest of the barriers (U_+ and U_-; see Fig. 9(a)) for those transitions should be maximized. Since it happens exactly at $V_1=V_{eq}$, where $U_+=U_-=U$, we have given special attention to this point in our numerical experiments. For this particular circuit, the maximum energy barrier (in temperature units) is $U=5.1$ K.

TABLE III. Possible scenarios for a single electron entering the trap: (A) electron (+1) moves in; (B) hole (−1) moves out, leaving an electron in the trap.

Island #	6	7	8	9	10	11	12	13
	0	0	0	0	0	0	0	0
	1	0	0	0	0	0	0	0
	0	1	0	0	0	0	0	0
	...	...	...	...	...	...	...	...
	0	0	0	0	0	0	1	0
	0	0	0	0	0	0	0	1
				(A)				
	0	0	0	0	0	0	0	0
	0	0	0	0	0	0	-1	1
	0	0	0	0	0	-1	0	1
	...	...	...	...	...	...	...	...
	-1	0	0	0	0	0	0	1
	0	0	0	0	0	0	0	1
				(B)				

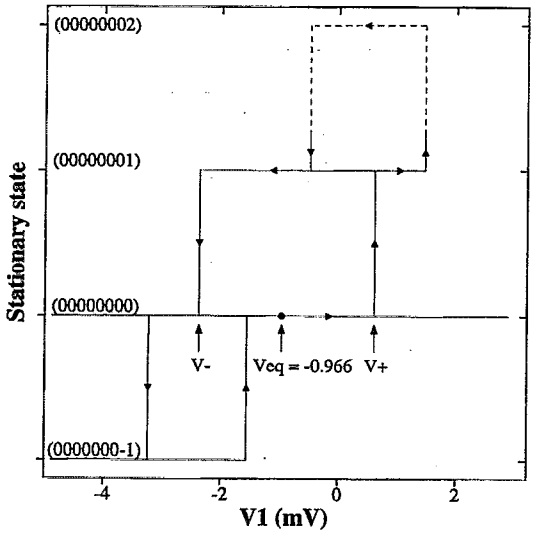

FIG. 10. Phase diagram of the 8-junction trap at the optimal potential $V_2 = V_{opt} = -8.57$ mV, which maximizes the bistability loop width $\Delta V = V_+ - V_-$ and the energy barrier height at the equilibrium point $V_1 = V_{eq}$. The dashed line shows the next bistable loop schematically; in fact, it has a complex fine structure corresponding to several charge states. Numbers in parentheses show electron configurations of the states (island 6 on the left, island 13 on the right).

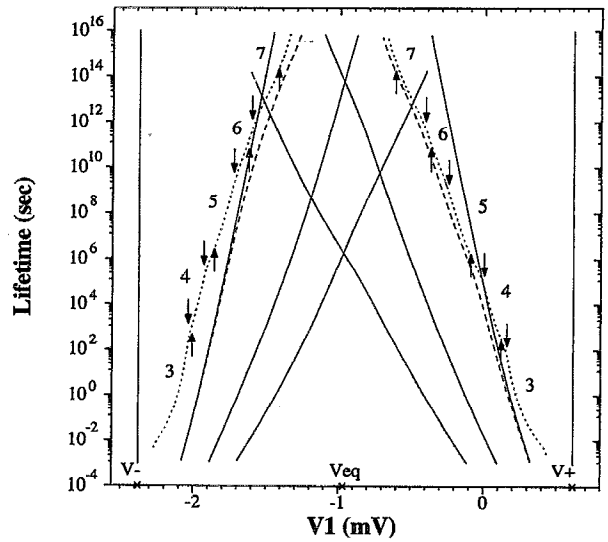

FIG. 11. Lifetimes of the static states of the 8-junction trap for different temperatures. The curves with negative (positive) slope describe the lifetime of the empty (full) cell. Solid lines: classic approximation for $T=0$ (vertical lines), 50, 100, and 150 mK. Dotted lines: cotunneling included, $T=0$. Dashed lines: cotunneling included, 50 mK. At 100 mK and 150 mK, the results including cotunneling practically coincide with the classic ones. Arrows pointing down mark the voltages at which transitions at different cotunneling orders (indicated by the numbers surrounding the arrows) have the same rates. Arrows pointing up mark the voltage at which the lowest of these cotunneling orders becomes possible.

Due to the stray capacitances of the islands, the energy profiles are not only dependent on the potential difference $V_1 - V_2$, but also on V_2. In particular, the energy barrier height U in the equilibrium point V_{eq} is maximum at a certain optimal value $V_2 = V_{opt}$ (Fig. 9(a) shows the energy profiles obtained using this optimal value). The voltage width of the bistable region $\Delta V = V_+ - V_-$ is maximum in the vicinity of the same $V_2 = V_{opt}$.

Figure 10 shows the phase diagram of the system, i.e. the boundaries of its possible stationary charge states (for a fixed voltage $V_2 = V_{opt}$). Notice that, at $V_1 \sim V_{eq}$, there are only two possible states (we will refer to them as 0 and 1 for the sake of simplicity). Closer to the boundaries of the main bistable loop, other states are also possible, though they have larger energies and are rather metastable.

C. State lifetimes

Even within the bistable loop $[V_-, V_+]$, thermal fluctuations and cotunneling may result in spontaneous switchings $0 \to 1$ and $1 \to 0$. Our first goal was to use SENECA to find the rates $\Gamma_\pm$ of these switching events (i.e. the corresponding lifetimes $\tau_\pm = 1/\Gamma_\pm$). The results of such calculation are shown in Fig. 11. It can be seen, first of all, that at relatively high temperatures ($\sim$ 100 mK and above), the results of calculations with and without account of cotunneling virtually coincide. This means that the main mechanism of spontaneous switching at those temperatures is the classical thermally activated hopping over the energy barrier. If the lifetime is relatively large ($\tau \gg C/G$, where C and G are typical scales for capacitances and conductances of the system, respectively), it may be determined using the "discrete" version[11] of the usual Kramers formula:

$$\tau \approx \frac{e^2}{G} \frac{\Delta U_+ + \Delta U_-}{\Delta U_+ \Delta U_-} \exp(U/k_B T), \tag{21}$$

where ΔU_+ and ΔU_- characterize the shape of the top of the energy barrier (Fig. 9(a)). Because the barrier height U is an almost linear function of the potential V_1, in semilog plot the $\tau_\pm(V_1)$ dependencies are also almost linear. Small deviations from linearity are mostly due to the discreteness of the barrier. Indeed, the barrier maximum switches from island to island as V_1 changes, resulting not in an exactly straight line, but in a piecewise linear curve (Fig. 11).

At lower temperatures, cotunneling gradually becomes the main mechanism of spontaneous switching. An important feature is that lifetimes diverge at $V = V_{eq}$ as $T \to 0$. This is a direct consequence of the fact that, at $T=0$, cotunneling between two states with the same energy vanishes (as expressed by Eqs. (4) and (8)).

Another feature in Fig. 11 is the oscillatory behavior of the cotunneling curves at low temperatures. This results from the change of the dominating cotunneling order with V_1, and the different dependencies of the rates on V_1 for different orders of cotunneling. The dominating cotunneling orders in each region of Fig. 11 are given by the numbers following the cotunneling curves at $T=0$. The arrows pointing up mark voltages V_1 at which cotunneling in lower order becomes possible. The arrows pointing down mark voltages at which cotunneling in this lower order acquires a rate equal to that in the previously dominating order. The separation between corresponding up and down arrows increases with the order of transition, confirming our earlier predictions (see Sec. II).

TABLE IV. Capacitance matrix of the 6-junction trap (in 10^{-16} Farad).

Elec./ sl. #	Island number 6	7	8	9	10	11	12	13
0	4.07×10^{-2}	1.60×10^{-2}	4.13×10^{-2}	1.19×10^{-2}	1.55×10^{-1}	1.09×10^{-1}	1.81×10^{-1}	1.71×10^{-1}
1	$1.90\times10^{+0}$	2.37×10^{-2}	2.72×10^{-2}	9.37×10^{-3}	4.03×10^{-2}	2.60×10^{-2}	1.51×10^{-2}	1.76×10^{-2}
2	8.28×10^{-3}	4.16×10^{-3}	1.12×10^{-2}	5.79×10^{-3}	5.77×10^{-2}	1.13×10^{-1}	2.17×10^{-2}	3.88×10^{-2}
3	2.05×10^{-2}	8.35×10^{-3}	1.75×10^{-2}	6.96×10^{-3}	4.89×10^{-2}	2.95×10^{-2}	$2.77\times10^{+0}$	8.43×10^{-2}
4	9.42×10^{-3}	4.08×10^{-3}	8.95×10^{-3}	3.85×10^{-3}	2.65×10^{-2}	2.07×10^{-2}	$2.93\times10^{+0}$	1.24×10^{-1}
5	6.14×10^{-3}	2.97×10^{-3}	7.17×10^{-3}	3.44×10^{-3}	3.10×10^{-2}	3.79×10^{-2}	5.13×10^{-2}	1.39×10^{-1}
6		$1.90\times10^{+0}$	2.07×10^{-2}	3.19×10^{-3}	1.06×10^{-2}	4.66×10^{-3}	2.36×10^{-3}	2.25×10^{-3}
7			$1.90\times10^{+0}$	8.93×10^{-3}	6.36×10^{-3}	2.97×10^{-3}	1.19×10^{-3}	1.16×10^{-3}
8				$1.90\times10^{+0}$	3.12×10^{-2}	8.65×10^{-3}	3.09×10^{-3}	2.90×10^{-3}
9					$1.90\times10^{+0}$	1.23×10^{-2}	1.46×10^{-3}	1.44×10^{-3}
10						$4.28\times10^{+0}$	2.88×10^{-2}	2.53×10^{-2}
11							2.07×10^{-2}	3.32×10^{-2}
12								2.75×10^{-1}

The oscillations are quickly smoothed out as the temperature is raised (above $\sim$ 50 mK in this particular case).

Looking at the absolute numbers, we see that the rate of spontaneous switching in the 8-junction trap may be extremely low: lifetimes in excess of 10^{16} s (i.e., $\tau \geqslant 10^{26} C/G$) are possible at achievable temperatures ($\sim$ 50 mK) within a relatively broad parameter window. While for digital devices such high stability may be necessary, for other applications it may be traded for the device simplicity. For example, a combination of two single electron traps gives another important device, the N-junction turnstile,[5] which may serve as a dc current standard. For devices of this type, lifetimes of the order of 10^4 s would be completely acceptable for present-day metrology, providing a relative error of the order of 10^{-10}. Thus, we will not proceed in the analysis of the 8-junction device, but instead we will discuss the second device, a 6-junction trap.

The 6-junction trap was obtained by merely short-circuiting two junctions of the 8-junction system (see Table IV for the capacitance matrix). Figure 12(b) shows the phase diagram of the trap at $V_2 = V_{opt}$; the maximum barrier height is $U = 3.7$ K.

Figure 13 shows the lifetimes of the states 0 and 1 in the 6-junction trap as a function of the applied voltage for different temperatures. As in the 8-junction device, oscillations due to the change in the dominating cotunneling order can be observed in the curves obtained at $T = 0$ and 50 mK, though the effect is somewhat smoothed in the latter case. Even though lifetime is completely determined by classic activation at 100 mK and 150 mK, cotunneling is quite significant at 50 mK and below.

The most important difference between the 8-junction and the 6-junction traps is the order of magnitude of the lifetimes. Figure 14 shows that difference in more detail, as the lifetimes of both circuits at $V_1 = V_{eq}$ are plotted against the inverse temperature. As the temperature lowers, thermal activation is abruptly replaced by cotunneling as the main source of error. The inset, showing the crossover on a smaller scale, demonstrates that in fact the transition occurs smoothly, though within a very narrow range of tempera-

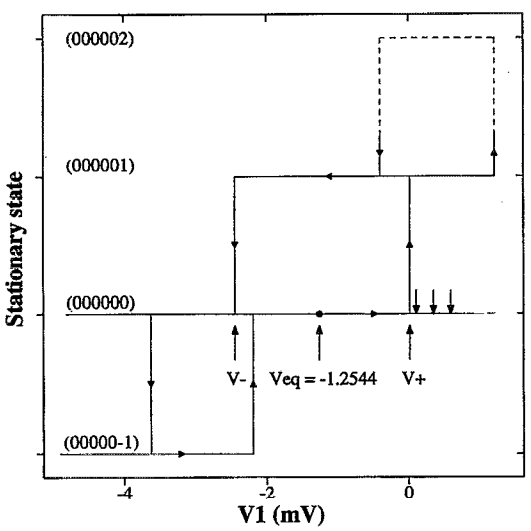

FIG. 12. Phase diagram of the 6-junction trap at $V_2 = V_{opt} = -10.0$ mV. Dashed line is a schematic description (see caption to Fig. 10).

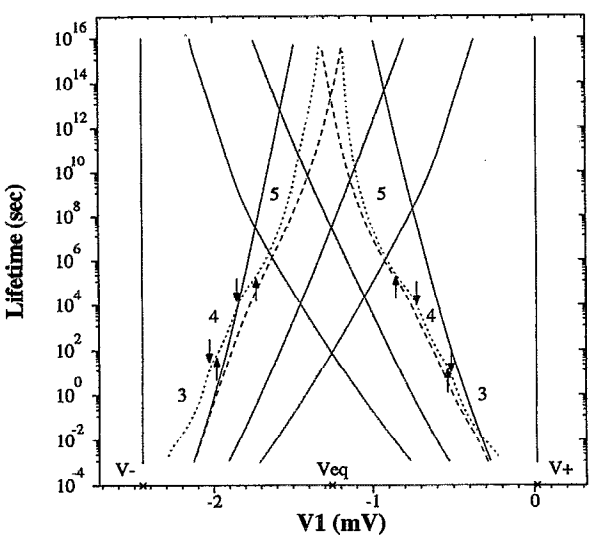

FIG. 13. Lifetimes of the static states of the 6-junction trap for different temperatures. The notation is similar to that in Fig. 11.

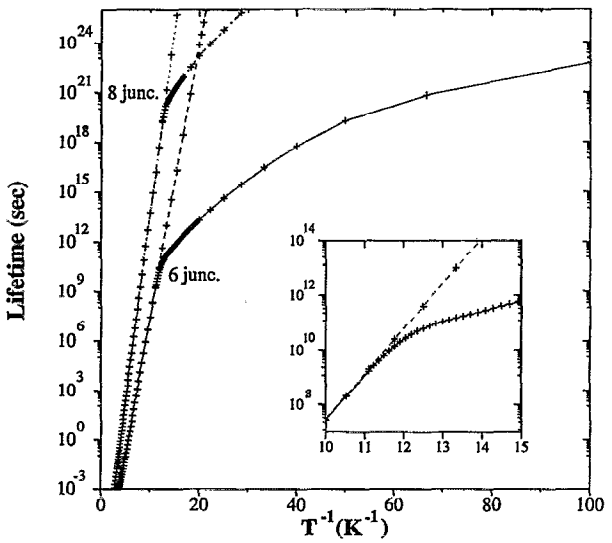

FIG. 14. Lifetime at $V_1 = V_{eq}$ and $V_2 = V_{opt}$ as a function of temperature for the 6- and 8-junction traps. Results of the 6-junction trap: solid line — cotunneling included; dashed line — classic. Results for the 8-junction trap: dot-dash line — cotunneling included; dotted line — classic. The inset shows the split of the cotunneling and classic curves of the 6-junction trap.

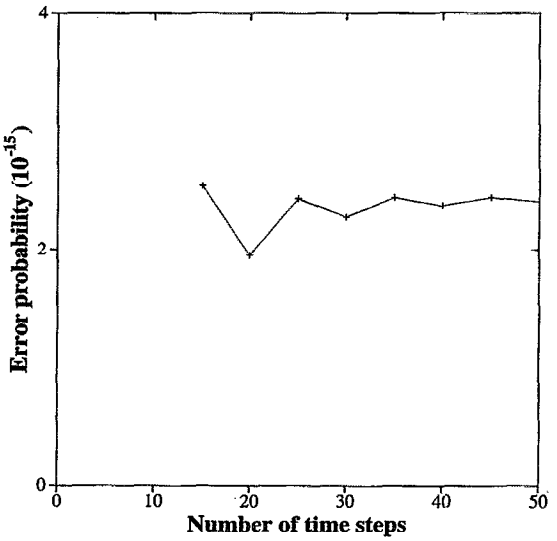

FIG. 15. Convergence of the error probability with the number of time steps, at $\zeta = 6 \times 10^3\ RC$, $A = 1.6$ mV, and $T = 100$ mK, for the $0 \rightarrow 1$ switching.

tures. The comparison of the curves for the two traps shows that decreasing the number of junctions by two increases the error probability by approximately 6 orders of magnitude at 100 mK, and by about 10 orders of magnitude at 50 mK. These curves agree in order of magnitude with the theoretical estimates of thermal activation (see Eq. (3)) at 100 mK, and cotunneling at 50 mK.[5]

D. Dynamic errors

In order to analyze the induced switching between the stable states of the 6-junction trap, we have studied the results of the application of a voltage pulse to a trap previously biased at the equilibrium point V_{eq}. The pulse used was of the form

$$V_1(t) = V_{eq} + A/2(1 - \cos(2\pi t/\zeta)), \quad 0 \leq t \leq \zeta, \qquad (22)$$

where the pulse amplitude A should be larger than $|V_{\pm} - V|$ (see Fig. 12). The error in this type of operation is the conservation of the initial state (or any state on the same side of the energy barrier) at $t = \zeta$. We have studied the error probability as a function of the signal duration ζ, amplitude A of the applied pulse, and temperature. As we have mentioned before, SENECA breaks the period ζ into a number of time steps. Figure 15 shows a typical error probability (for $\zeta = 6 \times 10^{-7}$ s, $A = 1.60$ mV, $T = 100$ mK) as a function of the number of time steps. Based on that plot (and similar ones taken at different values of ζ), we have concluded that 25 time steps are quite sufficient for the accuracy we need.

Figure 16 shows the error probability of the $0 \rightarrow 1$ switching at $T = 0$, as a function of the pulse duration ζ for three different pulse amplitudes (see the three arrows pointing down in Fig. 12, which show the maximum potential reached by each of the three pulses). The error rate would be an approximate exponential function of the difference $(A + V_{eq} - V_+)$ if the pulse were a square wave. In this case, the vertical distances between neighboring curves in Fig. 16 would be the same. In our curves these distances differ by $\sim 60\%$, as a result of the cosine wave used.

Figure 17(a) shows the error probability of the $0 \rightarrow 1$ switching at a fixed pulse amplitude $A = 1.6$ mV, as a function of the pulse duration ζ for different temperatures. All four curves are straight lines, up to some value of ζ. Indeed, the linear part results from the dynamic error of the trap which did not have time enough to switch, holding some probability of the initial state 0 at the end of the period. Numerical simulations show that, for our parameters, the dominating channel of decay of state 0 starts with a single electron moving from wire 1 to the first island of the array (6 in our notation). This initial event is the bottleneck of the switching process, because it corresponds to the smallest en-

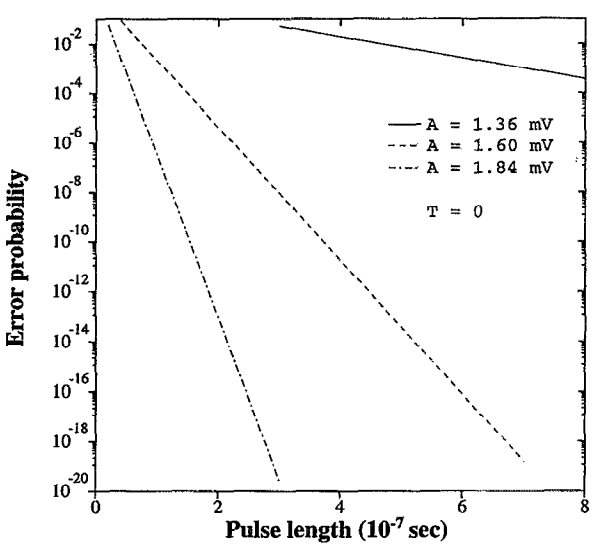

FIG. 16. Error probability as a function of the switching pulse duration for different signal amplitudes (see arrows in Fig. 12), in the 6-junction trap.

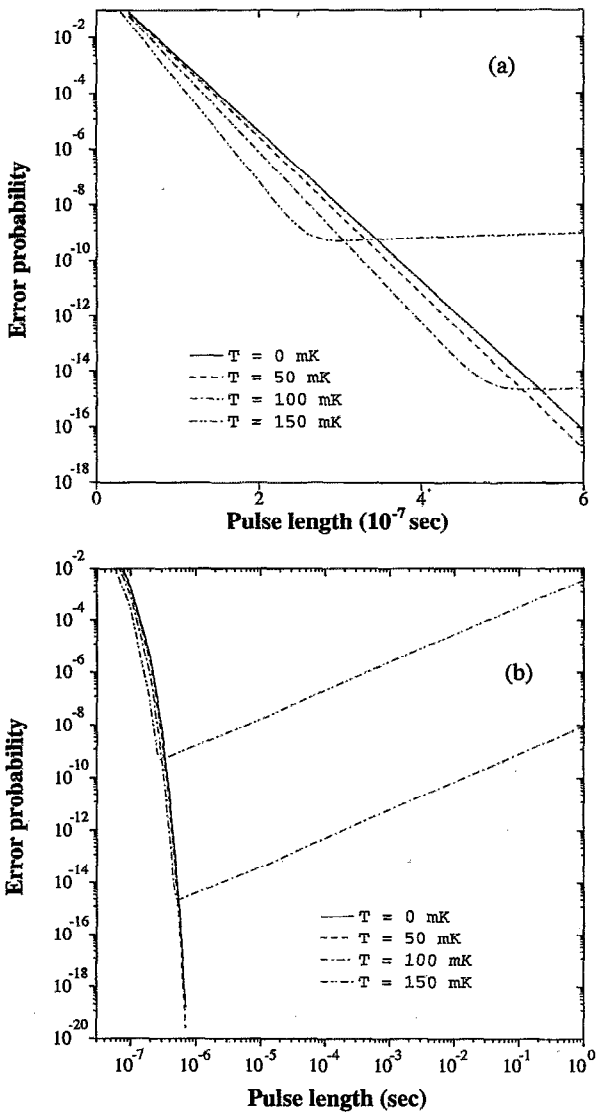

FIG. 17. Error probability vs pulse duration in the 6-junction trap, for different temperatures at $A = 1.6$ mV: (a) linear scale of ζ, showing the exponential behavior at small ζ; (b) logarithmic scale of ζ, showing the linear behavior at large ζ.

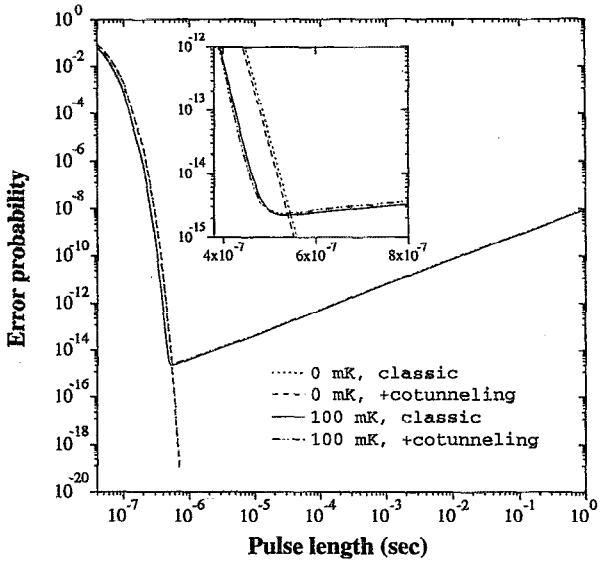

FIG. 18. Effect of cotunneling on the dynamic error probability. The inset shows the region of the turning point of the 100 mK curve.

ergy difference between islands. Hence, the decay dynamics may be fairly described by Eq. (1) with only one nonvanishing rate $\Gamma_{1\to6}(t)$. In this approximation, the error probability is an exactly exponential function of ζ. In this exponential range, temperature accelerates the switching process, providing energy for the electron to cross the barrier before it is completely lifted.

As we move to longer periods, however, the probability of error starts to grow with the pulse duration (Fig. 17(b)). The reason for this behavior is the reverse switching ($1\to0$) after the initial switching ($0\to1$) has occurred. This process is specially probable during the tail of the pulse, when $V_1(t)\to V_{eq}$ and the energy barrier for the reverse switching is the lowest. Here the error probability grows linearly with time because, since $dV(t)/dt\to0$ as $t\to\zeta$, the rate of the reverse switching is almost constant in time. Due to the exponential character of the error probability at shorter periods, the transition from the temperature-assisted to the temperature-disturbed operation occurs in a very narrow range of ζ.

Finally, Fig. 18 shows the effect of cotunneling on the $0\to1$ switching operation at $T=0$ and 100 mK. Note that cotunneling speeds up the device operation and thus reduces the dynamic errors. This happens because cotunneling, like thermal activation, allows the electron to hop over the barrier before the classical $0\to1$ switching point $V_1 = V_+$ is reached. After the error probability curve turns up at some ζ (and $T \neq 0$), the cotunneling curve crosses the classic one, increasing the error probability. Note that although the program could capture cotunneling effects during the switching

TABLE V. Memory and CPU time requirements for the calculation of lifetime for the 6- and 8-junction traps in one bias point. The two numbers in each column are the minimum and maximum requirements over all points shown in Figs. 11 and 13.

	6 junctions				8 junctions			
	0 mK	50 mK	100 mK	150 mK	0 mK	50 mK	100 mK	150 mK
CPU time (s)	1–2	2–6	15–40	25–570	70–280	100–610	90–1200	610–4200
Memory (Mbytes)	1.0–1.1	1.0–1.5	1.5–2.5	3.0–10.5	1.0–3.0	1.5–5.5	2.5- -10.0	6.5–55.0

TABLE VI. Memory and CPU time requirements for the calculation of dynamic error of the 6-junction trap. The two numbers in each column are the minimum and maximum requirements over all points, shown in Fig. 17. The columns marked by (*) include cotunneling.

	0 mK (*)	50 mK	100 mK (*)	150 mK
CPU time (s)	6–1800	30–120	60–9000	70–990
Memory (Mbytes)	1.5–12.0	2.5–3.0	3.5–90.0	4.0–8.5

operation, their influence on the dynamic error probability is practically negligible.

V. CONCLUSION

We introduced SENECA, a new program for the calculation of probabilities of rare events in single electron systems, capable of analysis of circuits with arbitrary topology and parameters. It can find states with probabilities as small as desired, against the background of a large number of states with larger probabilities. The usefulness of the program has been demonstrated by a numerical study of single electron traps.

SENECA is a C program written, currently, for use on UNIX-based workstations. In order to show the computer requirements, we made some measurements using a Silicon Graphics INDIGO 2. Table V shows the approximate maximum and minimum CPU time and memory (per point) taken over several points of Figs. 11 and 13, required for the determination of lifetimes of the static states of the 6- and 8-junction traps. Notice that both time and memory grow rapidly with increasing temperature. Table VI shows the resources required for the analysis of dynamic errors in the 6-junction trap (see Figs. 17 and 18). Because the processes taken at $T=0$ and 100 mK in Table VI include cotunneling, their corresponding computer requirements are much more demanding. The two tables show that, for simple devices in a considerable range of parameters (such as low temperature), personal computers can be successfully used to run this code. In the case of more complex geometries involving many devices and a wide range of parameters, workstations may not be powerful enough and supercomputers may become a necessity.

Our future plans are to use SENECA for the study of more complex single electron devices and circuits, such as dc current standards, as well as for the analysis of background charge fluctuations[5] which have been neglected so far.

ACKNOWLEDGMENTS

Numerous fruitful discussions with D. Averin, P. Dresselhaus, R. Chen, K. Matsuoka, and J. Lukens, and technical help by A. Grossi are gratefully acknowledged. The work was supported in part by AFOSR Grant No. 91-0445 and ONR/ARPA Grant No. N00014-93-1-0880. One of the authors (L. F.) was supported by CNPq-Brazil.

[1] K. K. Likharev, J. Res. Develop. **32**, 144 (1988).
[2] D. V. Averin and K. K. Likharev, in *Mesoscopic Phenomena in Solids*, edited by B. Altshuler (Elsevier, Amsterdam, 1991), p. 173.
[3] *Single Charge Tunneling*, edited by H. Grabert and M. H. Devoret (Plenum, New York, 1992).
[4] K. K. Likharev and V. K. Semenov, *Extended Abstracts, International Superconducting Electronics Conference* (ISEC, Tokyo, 1987), p. 182.
[5] D. V. Averin and K. K. Likharev, in *Single Charge Tunneling*, edited by H. Grabert and M. H. Devoret (Plenum, New York, 1992), p. 311.
[6] K. Nakazato and J. D. White, *Proc. of IEDM'92* (IEEE, New York, 1992), pp. 487–490.
[7] P. D. Tougaw and C. S. Lent, J. Appl. Phys. **75**, 1818 (1994).
[8] R. Chen, K. Matsuoka, and K. K. Likharev (unpublished).
[9] K. K. Likharev, N. S. Bakhvalov, G. S. Kazacha, and S. I. Serdyukova, IEEE Trans. Magn. **25**, 1436 (1989).
[10] H. Pothier, Ph.D. thesis, University of Paris 6, 1991.
[11] H. D. Jensen and J. M. Martinis, Phys. Rev. B **46**, 13407 (1992).
[12] D. V. Averin, A. A. Odintsov, and S. V. Vyshenskii, J. Appl. Phys. **73**, 1297 (1993).
[13] D. V. Averin and A. A. Odintsov, Phys. Lett. A **140**, 251 (1989).
[14] A different mechanism, the so-called elastic cotunneling (see Ref. 15), is also possible, but its rate is negligibly low in metallic structures (see Ref. 16).
[15] L. I. Glazman and K. A. Matveev, Sov. Phys.-JETP **71**, 1031 (1990).
[16] D. V. Averin and Yu. V. Nazarov, Phys. Rev. Lett. **65**, 2446 (1990).
[17] A. N. Korotkov, D. V. Averin, K. K. Likharev, and S. A. Vasenko, in *Single-Electron Tunneling and Mesoscopic Devices*, edited by H. Koch and H. Lubbig (Springer, Berlin, 1992), p. 45.
[18] Y. V. Nazarov, J. Low Temp. Phys. **90**, 77 (1993).
[19] P. Lafarge and D. Esteve, Phys. Rev. B **48**, 14309 (1993).
[20] H. Schoeller and G. Schon, *Mesoscopic quantum transport: Resonant tunneling in the presence of strong Coulomb interaction*, preprint (1994).
[21] Actually, in order to account for a possible inaccuracy of the estimate $P_{\rm est}$, $P_{\rm th}(n)$ is decreased by five orders of magnitude if it drops below $P_{\rm th}$, and one more iteration is performed with that value.
[22] G. H. Golub and C. F. Van Loan, *Matrix Computations* (Johns Hopkins University Press, Baltimore, 1989), pp. 555–560.
[23] T.A. Fulton, P.L. Gammel, and L.N. Dunkleberger, Phys. Rev. Lett. **67**, 3148 (1991).
[24] M.H. Devoret, D. Esteve, and C. Urbina, Nature **360**, 547 (1992).
[25] P.D. Dresselhaus, L. Ji, J.E. Lukens, and K.K. Likharev, Phys. Rev. Lett. **72**, 3226 (1994).
[26] J.E. Lukens, P.D. Dresselhaus, S. Han, L. Ji, K.K. Likharev, and W. Zheng, Physica B (to be published).
[27] Courtesy of Kenji Matsuoka. The calculations were performed using the FastCap package (courtesy of Jacob White, MIT) complemented by a special program for automatic paneling of the interfaces.